Communication

State mixing by spin-orbit coupling in the anionic chloroiodine dissociations

Xia, L.; Wang, X. D.; Xuan, C. J.; Zeng, X. J.; Li, H. K.; Tian, S. X.; Pan, Y.; Lau, K. C.

Published in:
Journal of Chemical Physics

Published: 01/01/2014

Document Version:
Final Published version, also known as Publisher's PDF, Publisher's Final version or Version of Record

Published version (DOI):
10.1063/1.4862684

Publication details:
Xia, L., Wang, X. D., Xuan, C. J., Zeng, X. J., Li, H. K., Tian, S. X., Pan, Y., & Lau, K. C. (2014). Communication: State mixing by spin-orbit coupling in the anionic chloroiodine dissociations. *Journal of Chemical Physics*, *140*(4), Article 41106. https://doi.org/10.1063/1.4862684

Communication: State mixing by spin-orbit coupling in the anionic chloroiodine dissociations

Cite as: J. Chem. Phys. **140**, 041106 (2014); https://doi.org/10.1063/1.4862684
Submitted: 03 November 2013 • Accepted: 07 January 2014 • Published Online: 27 January 2014

L. Xia, X.-D. Wang, C.-J. Xuan, et al.

Communication: State mixing by spin-orbit coupling in the anionic chloroiodine dissociations

L. Xia,[1] X.-D. Wang,[1] C.-J. Xuan,[1] X.-J. Zeng,[1] H.-K. Li,[1] S. X. Tian,[1,a)] Y. Pan,[2] and K.-C. Lau[2,a)]

[1]*Hefei National Laboratory for Physical Sciences at the Microscale, Department of Chemical Physics, University of Science and Technology of China, 96 Jinzhai Road, Hefei, Anhui 230026, China*
[2]*Department of Biology and Chemistry, City University of Hong Kong, 83 Tat Chee Avenue, Kowloon, Hong Kong, China*

(Received 3 November 2013; accepted 7 January 2014; published online 27 January 2014)

Three spin-orbit states, $1^2\Pi_{1/2}$, $2^2\Pi_{3/2}$, and $2^2\Pi_{1/2}$, of chloroiodine anion (ICl^-) formed by low-energy electron attachment in the Franck-Condon region are associated with the dissociative limits of I^- ($^1S_0$) and Cl ($^2P_{3/2}$) or Cl* ($^2P_{1/2}$) fragments. Within the adiabatic scheme, the presumptive Π-symmetry of the fragment angular distributions is dramatically changed to be the Π-Σ mixing symmetry, due to the significant spin-orbit interaction effect on the electronic state couplings of ICl^-. The present experimental approach also enables us to separate the contributions of different electronic states from the mixed states, providing a crucial method for quantitatively evaluating the configuration-interaction wavefunctions. © *2014 AIP Publishing LLC*. [http://dx.doi.org/10.1063/1.4862684]

Spin-orbit (SO) coupling is known to cause many novel phenomena in electronic materials,[1] while its fundamental knowledge stemmed from the electron behaviors in atoms and molecules.[2] Within the Born-Oppenheimer approximation, the SO coupling can lead to the adiabatically mixed electronic states and some striking phenomena, e.g., the SO decay selectivity of O_2 at autoionization-states[3] and the unexpected long lifetime of doubly charged cation CO^{2+},[4] that were interpreted qualitatively with configuration-interaction (CI) calculations considering the SO perturbation (by introducing the Breit-Pauli operator H_{SO}).[5] In the molecular photoabsorption and the atom-molecule collision, the electronic state mixing is frequently exhibited as the specific anisotropic angular distribution of fragment or product, which arises from either the adiabatically SO coupling, the diabatic intersystem-crossing of the potential energy surfaces, or both.[6] The second mechanism, distinctly different from the former, is beyond the Born-Oppenheimer approximation.

These two dynamic processes are usually observed together for a certain molecule.[6] However, very few reports are only concentrated in the molecular adiabatic SO coupling. Electron-molecule resonance formed by the low-energy electron attachment provides a suitable vessel for such study, in particular, when the SO-induced mixing magnitude between two resonant states with a same Ω (the projection of the total angular momentum onto the internuclear axis) is larger than the nonadiabatic coupling.[7] The SO-induced Σ-Π state mixing was proposed to increase for diatomic anions from HCl^-, HBr^-, to HI^-.[7–9] In contrast, nonexistence of this Σ-Π state mixing was proposed in the dissociative electron attachment (DEA) to chloroiodine (ICl),[10] which was subsequently disputed by a CI computational study.[11] The strong state mixing, if existed in this DEA process, can be definitely reflected on the fragment angular distributions, but demanding the high sensitivity of the measurements. The previous experimental studies using the traditional rotating ion detector within a turn-table arrangement[8,10] could only provide the angular distribution in a limit angle (θ) range, thereby their conclusions sometime took a part as whole. Here we report a DEA study of ICl using anion time-slice velocity map imaging (VMI) technique. The state-of-the-art VMI technique enables us to identify different anionic fragments of the DEA process and record the angular distribution of a specific fragment in the full range $\theta = 0 = 2\pi$.[12–16]

In the Franck-Condon region of the vertical electron attachment, various resonant states of ICl^- are accessible. The potential energy curves of both the neutral ICl at the ground state and the anion ICl^- at the low-lying resonances were recalculated with the internally contracted multi-reference CI method including the SO coupling.[17] According to atomic electron affinities and the SO splitting energies of two ^2P states of Cl and I atoms, the dissociation pathways are depicted in Fig. 1. Considering Hund's case (a) for the SO coupling of ICl^- and the predominant eigenstate $|\Phi\rangle$ of the CI wavefunction $|\Psi_{CI}\rangle$ in the Franck-Condon region, each $^2\Pi$ state splits into $^2\Pi_{3/2}$ and $^2\Pi_{1/2}$, and they together with two $^2\Sigma_{1/2}{}^+$ states are assigned as the resonant states of ICl^-. Without the SO coupling, these states contract into two bound states Σ and Π, and two nearly dissociative states Π* and Σ*.[11] According to the Wigner-Witmer correlation rules and symmetry conservation, the following dissociations are permitted: $ICl^-(^2\Pi_{3/2}) \rightarrow I^-(^1S_0) + Cl(^2P_{3/2})$; $ICl^-(^2\Pi_{1/2}) \rightarrow I^-(^1S_0) + Cl^*(^2P_{1/2})$; $ICl^-(^2\Sigma_{1/2}) \rightarrow I^-(^1S_0) + Cl(^2P_{3/2})$ or $Cl^-(^1S_0) + I(^2P_{3/2})$. However, one can find another two irregular processes: $ICl^-(1^2\Pi_{1/2}) \rightarrow I^-(^1S_0) + Cl(^2P_{3/2})$ and $ICl^-(2^2\Sigma_{1/2}{}^+) \rightarrow Cl^-(^1S_0) + I^*(^2P_{1/2})$, implying that the SO

a)Authors to whom correspondence should be addressed. Electronic addresses: sxtian@ustc.edu.cn and kaichung@cityu.edu.hk.

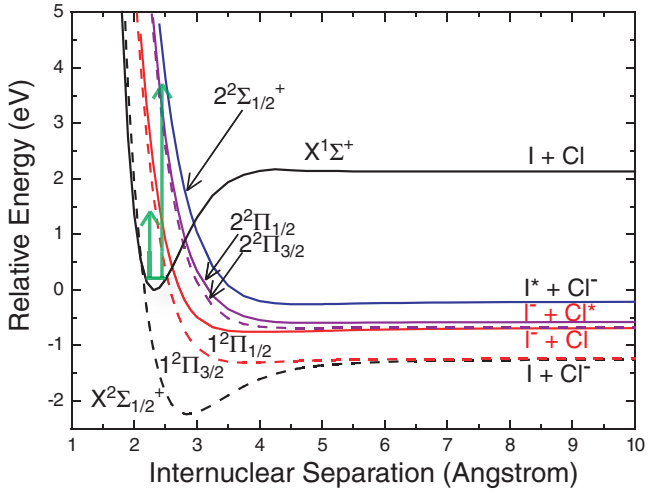

FIG. 1. Potential energy curves of the ground-state ICl and the anion ICl^- at the low-lying states. I* and Cl* represent the species at the higher SO state $^2P_{1/2}$, while I and Cl are at the lower $^2P_{3/2}$ state. The ground state of I^- (or Cl^-) is $^1S_0$. The spectroscopic term (Σ or Π) assigned in the Franck-Condon region is determined with the predominant eigenstate of the CI wavefunctions; the vertical arrows denote different attachment energies investigated in this work.

coupling rule in the asymptotic region is different from that in the Franck-Condon region.

The present experiments were done at the attachment energies, 1.2, 1.5, 1.8, 3.0, 3.7, and 4.5 eV, using our VMI apparatus.[12,13,17] The sliced images of I^- are depicted in Figs. 2(a)–2(f). At the low electron energies (see Figs. 2(a)–2(c)), the backward scattering distributions are predominant, while two weak petal-like distributions are around $\theta = 45^\circ$ and 315° (in the forward direction). The angular distributions are significantly changed at the higher electron energies (see Figs. 2(d)–2(f)), exhibiting the intensive ion signals in the direction perpendicular to the electron beam. Such remarkable image-pattern changes with the attachment energy were not observed for Cl^-. The dipole field of molecular target[10] and the polarized molecular local bond[16] would indeed introduce a forward-backward asymmetry of the angular distribution, but they cannot be responsible for the present image-pattern evolution with the electron energy. Since the angular distributions are primarily relevant to the symmetries of the resonant states in the Franck-Condon region,[8,10,12–16] all of these images should presumably show the typical up-and-down ($^2\Pi$ state) or backward-forward ($^2\Sigma$ state) distributions. Obviously, the present observations should be attributed to the anomalous dissociation dynamics which will be elucidated in the following parts.

On the other hand, one can find that the image size (i.e., the ion kinetic energy or velocity) increases with the attachment energy. As shown in Fig. 2(g), the kinetic energy of I^- ion with the highest intensity is plotted against the electron energy, exhibiting a linear correlation. The extrapolation value as the intercept at the ordinate is about 0.21 eV which is the lowest kinetic energy of I^- gained from the exothermic dissociation $ICl + e^-(0\ eV) \rightarrow I^- + Cl$ (or Cl^*). Alternatively, this lowest kinetic energy of I^- can be calculated with the thermochemical data: 0.17 (producing I^- plus Cl^*) or 0.20

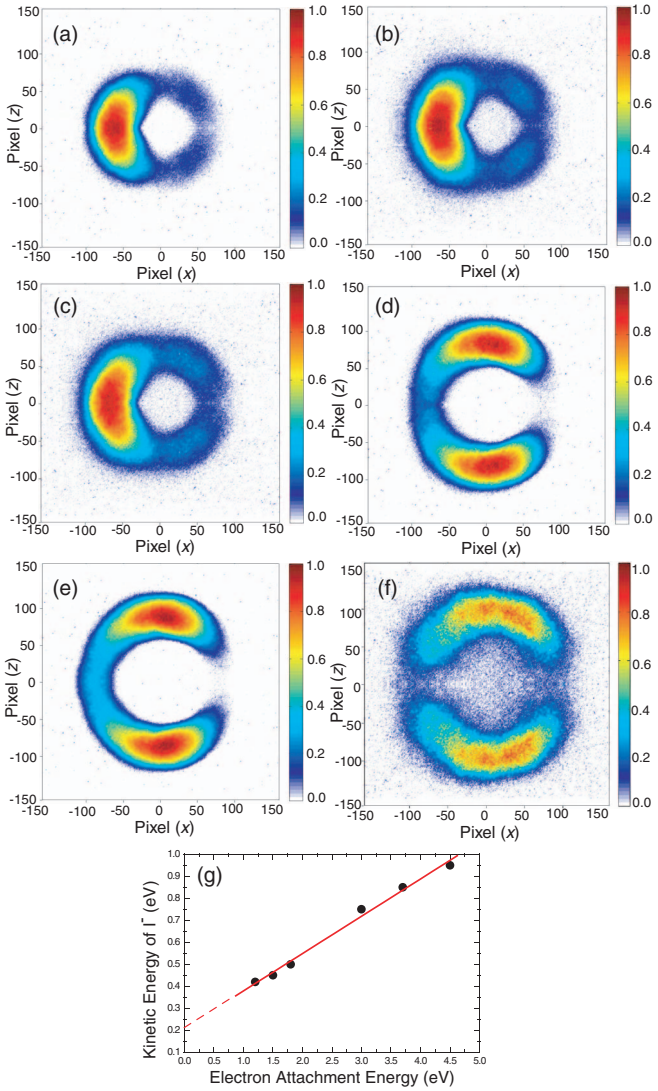

FIG. 2. Sliced images of I^- recorded at the electron energies of 1.2 (a), 1.5 (b), 1.8 (c), 3.0 (d), 3.7 (e), and 4.5 eV (f); and the measured kinetic energy of I^- as a function of the electron energy (g). In (a)–(f), the electron incident direction is from left to right and through the image center, and the anion intensity is normalized respectively.

(producing I^- plus Cl) eV. These two are in good agreement with the extrapolated value 0.21 eV.

The angular distribution of I^- is obtained by the ion signal integral of the selected annular area in each image.[17] The present experimental data (solid circles) together with those (empty circles) recorded by the rotating ion detector[10] are plotted in Fig. 4. Gratifying agreement between the present and previous[10] experiments can be found in Fig. 4(b); but some deviations are exhibited in Fig. 4(e), in particular, for the ion intensities around 30° and 110°.

The six electron energies selected here correspond to the energy positions of the low- and high-energy shoulders and the central peaks of two bands in the I^- yield spectrum.[10] Two resonant states in the Franck-Condon region were proposed: a narrow band centered at 1.45 eV was assigned as the DEA process relevant to $2^2\Sigma_{1/2}$ state; while a diffuse band at 3.7 eV was assigned to $^2\Pi$ state.[10] These assignments were based on the differential cross section measurements

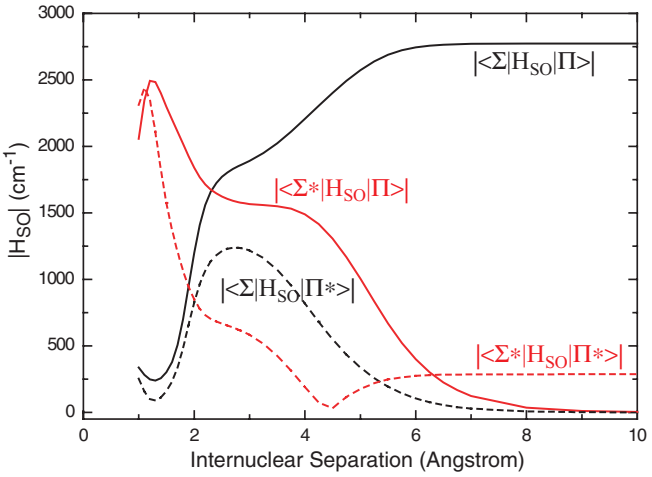

FIG. 3. Spin-orbit coupling matrix elements $|H_{SO}|$ as a function of the internuclear separation.

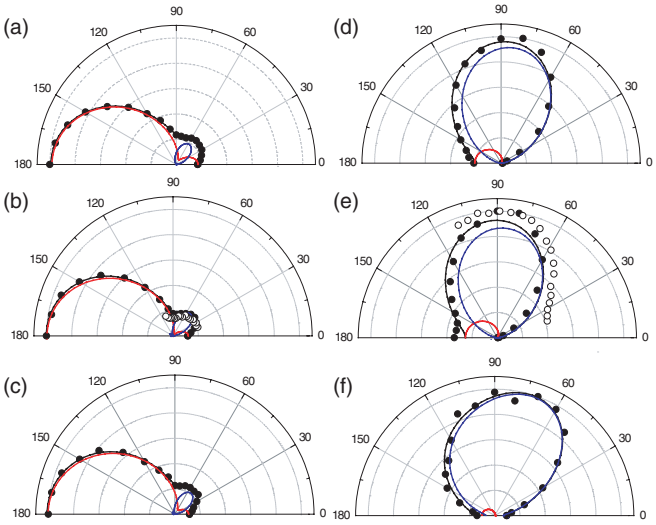

FIG. 4. Angular distributions (solid circles, this work; empty circles, from Ref. 10 after the normalizations) together with the experimental data fittings of I^- recorded at 1.2 (a), 1.5 (b), 1.8 (c), 3.0 (d), 3.7 (e), and 4.5 eV (f). Σ and Π components are colored, respectively, in red and blue; and their summarized curves are in black.

in the limited angle range $\theta = 20^\circ - 110^\circ$.[10] However, the authors also admitted that the $2^2\Sigma_{1/2}$ assignment was not in line with the previous studies (cited in Ref. 10). According to Maslen *et al.*[11] and our calculations, the resonant state at 1.45 eV should be $^2\Pi$, but this state strongly interacts with $\Sigma_{1/2}$ (Σ^*) state. These state-couplings further lead to the different state configurations in the asymptotic region ($R \rightarrow \infty$) with respect to those in the Franck-Condon region. The coefficients of Σ and Π components of the configuration state at the infinite internuclear separation obtained in this work are exactly the same as previous calculations.[11] The Π symmetry of two $^2\Pi_{3/2}$ states is entirely retained, $|\Psi_{CI}^{(1^2\Pi_{3/2}\ or\ 2^2\Pi_{3/2})}\rangle \xrightarrow{R\rightarrow\infty} |\Phi^{(\Pi\ or\ \Pi^*)}\rangle$ (the superscript denotes the predominant eigenstate in the Franck-Condon region or at the dissociative limit); while $|\Psi_{CI}^{(1^2\Pi_{1/2})}\rangle$ is transferred to a Σ-Π mixing state: $0.67|\Phi^{(\Sigma^*)}\rangle + 0.33|\Phi^{(\Pi^*)}\rangle$, and $|\Psi_{CI}^{(2^2\Pi_{1/2})}\rangle \xrightarrow{R\rightarrow\infty} 0.33|\Phi^{(\Sigma^*)}\rangle + 0.67|\Phi^{(\Pi^*)}\rangle$. These transformations arise from the SO interaction effect on the $^2\Pi$-$^2\Sigma$ state coupling with a change of the internuclear separation. The SO-induced Φ-Φ′ state coupling can be evaluated with the non-zero off-diagonal SO matrix elements ($|\langle\Phi|H_{SO}(R)|\Phi'\rangle|$).[2] In Fig. 3, the elements predicted in this work[17] exhibit the remarkable changes with the internuclear separation. Since the SO coupling of the heavy atom I is stronger than the L-molecular axis coupling at the dissociative limit,[2,9] Hund's case (a) for the SO coupling of ICl^- in the Franck-Condon region should be replaced with Hund's case (c)[2] at the dissociative limit.

To further elucidate the dissociation dynamics, we need to recall the basic theoretical model for the fragment momentum distribution in the DEA process of diatomic molecule,[18]

$$\sigma_{DEA} \propto \left| \sum_{l=\mu}^{\infty} i^l e^{i\delta_l} a(k)_{l\mu} Y_{l\mu}(\theta, \phi) \right|^2, \quad (1)$$

where k is the impinging electron wave vector and the impinging wave is further expressed with partial waves of different angular momenta l, azimuth angle ϕ equals zero degree for the central sliced image, $a(k)_{l\mu}$ is the weighing coefficient, $Y_{l\mu}$ is a spherical harmonics related to the initial (neutral) and resonant states, and δ_l is a potential scattering phase lag of a partial wave with angular momentum l. $|\mu|$ equals $|\Lambda_f - \Lambda_i|$, representing the difference in the projections of the total angular momenta Λ along the internuclear axis between the neutral and the resonant-state parent anion. In practice, the summation of the finite partial wave terms in Eq. (1) has been successfully applied.[13–16] Since the SO coupling was not considered in Eq. (1), here Λ is replaced with Ω. In the axial recoil approximation, the molecular rotations and ro-vibrational coupling are excluded. In the present case, the combination term with Σ ($\Lambda = 0$) and Π ($\Lambda = 1$) symmetries, rather than only Σ or Π, must be applied for the state mixing,

$$\sigma_{DEA} \propto I_1 + I_2 = \left| e^{i\delta_s} a_s Y_{00}(\theta) + i e^{i\delta_p} a_p Y_{10}(\theta) \right|^2 + \left| i e^{i\delta_{p'}} a_{p'} Y_{11}(\theta) - e^{i\delta_{d'}} a_{d'} Y_{21}(\theta) \right|^2, \quad (2)$$

where I_1 and I_2 terms represent the Σ- and Π-symmetry components, respectively; two partial waves with the angular momenta of $l = 0$ (s) and 1 (p) and $l = 1$ (p) and 2 (d) are adopted in each term.

Without the state mixing, considering the individual state $1^2\Pi$ or $2^2\Pi$ in the Franck-Condon region, these images should uniformly show the Π-symmetry feature, thus the angular distribution could be fitted well with the I_2 term (l can be extended from 1 to 3 or more). However, the experimental data fittings indicate that only the combination $I_1 + I_2$, rather than any one isolated term I_1 or I_2, gives the best results (see the black curves in Fig. 4, correlations ≥0.98). At the low energies (1.2, 1.5, and 1.8 eV, as shown in Figs. 4(a)–4(c), the red fitting curves (corresponding to the Σ-symmetry, I_1 term in Eq. (2) reproduce very well the

TABLE I. Fitting parameters of the I^- angular distributions and the composition percentages of $\sigma(\Pi^*$ or $\Sigma^*)$.

Attachment energy (eV)	1.2	1.5	1.8	3.0	3.7	4.5
a_s:a_p:$a_p{}'$:$a_d{}'$	1.00:1.05:0.68:0.38	1.00:1.19:0.60:0.64	1.00:0.99:0.53:0.55	1.00:0.58:3.42:0.16	1.00:0.58:3.02:0.11	1.00:0.87:6.13:2.09
δ_p-δ_s (rad)	2.55	3.10	3.13	3.13	3.06	3.13
$\delta_d{}'$-$\delta_p{}'$(rad)	0.00	0.28	0.00	0.00	0.66	1.29
Composition (%)		$\sigma(\Sigma^*)$			$\sigma(\Pi^*)$	
Expt.	84.4 ± 0.1	82.7 ± 0.1	83.4 ± 0.1	85.4 ± 1.6	82.0 ± 2.4	93.8 ± 0.9
Theor.[a]		80 (for $1^2\Pi_{1/2}$)			100 (for $2^2\Pi_{3/2}$) and 80 (for $2^2\Pi_{1/2}$)	

[a]Estimated with the weighing parameters of eigen wavefunctions in the asymptotic CI wavefunction.

strong backward scatterings; while the blue curves (corresponding to the Π-symmetry, I_2 term in Eq. (2) illustrate the weak forward scatterings. The weighing order between the Σ- and Π-symmetries is reversed for the angular distributions at the high electron energies. As shown in Figs. 4(d)–4(f), the Π-symmetry compositions are overwhelming, especially at 4.5 eV. The fitting parameters and the composition percentages are listed in Table I. The possibility about resonant-state interference[13] can be ruled out, because the $\pi/2$ phase-difference (φ) of the state orthogonality could be obtained if the superposition term ($2\sqrt{I_1 I_2}\cos\varphi$) was arbitrarily added in Eq. (2).

As mentioned above, $\left|\Psi_{\mathrm{CI}}^{R\to\infty}\right\rangle$ can be expanded with the eigen wavefunctions. If the angular-resolved differential cross section is assumed to be proportional to $\left\langle\Psi_{\mathrm{CI}}^{R\to\infty}\right|\left|\Psi_{\mathrm{CI}}^{R\to\infty}\right\rangle$, we can derive the contributions of individual eigenstates. Considering the orthogonality of these eigen wavefunctions, we estimated the Σ- or Π-symmetry composition percentages using the CI wavefunctions predicted in Ref. 11 and this work: 80% of the Σ-symmetry and 20% of the Π-symmetry for $1^2\Pi_{1/2}$, 20% of the Σ-symmetry and 80% of the Π-symmetry for $2^2\Pi_{1/2}$; and 100% of the Π-symmetry for $2^2\Pi_{3/2}$. In Table I, the composition percentages derived with the fitting parameters are 84.4% ± 0.1% (at 1.2 eV), 82.7% ± 0.1% (at 1.5 eV), and 83.4% ± 0.1% (at 1.8 eV) of the Σ-symmetry, where the uncertainty is determined by the respective fitting quality. All of these values are in line with the theoretical predictions, indicating again that the dissociations in the low energy range proceed via $1^2\Pi_{1/2}$ state (see Fig. 1), but the angular distributions are relevant to the configuration state at the large internuclear separation. At the high electron energies, the composition percentages derived with the fitting parameters are 85.4% ± 0.1% (at 3.0 eV), 85.4% ± 1.6% (at 3.7 eV), and 93.8% ± 0.9% (at 4.5 eV) of the Π-symmetry. As listed in Table I, these values fall into the theoretical scales, 100% (for $2^2\Pi_{3/2}$) and 80% (for $2^2\Pi_{1/2}$) of the Π-symmetry. As shown in Fig. 1, the dissociations in this high energy range proceed via $2^2\Pi_{3/2}$ and $2^2\Pi_{1/2}$ states. The percentage of the Π-symmetry, 93.8% ± 0.9% at the high energy of 4.5 eV obtained with the fitting results, is approximately equal to the theoretical value 100% for the lower state $2^2\Pi_{3/2}$; but the percentages at the low energies of 3.0 and 3.7 eV are close to 84.9% for higher state $2^2\Pi_{1/2}$. The energetic sequence is reversed, namely, we observed that the dissociative limit related to $2^2\Pi_{3/2}$ lied above that of $2^2\Pi_{1/2}$. Therefore, this attachment-energy dependent nonadiabaticity deserves further theoretical study, in particular, the dynamics beyond Born-Oppenheimer approximation should be treated explicitly.

In conclusion, we observed the Σ-Π mixing symmetries, rather than the pure Π symmetry determined by the resonant states in the Franck-Condon region, of the angular distributions of I^- fragment produced in the DEA to ICl. This is attributed to the resonant state couplings induced by the SO interactions that are varied with the internuclear separations. The Σ- and Π-symmetry composition ratios predicted with the CI wavefunctions at the dissociative limit are in good agreement with the respective contributions derived from the experimental data fittings, indicating a promising way to evaluate the quality of CI wavefunction calculations.

This work is supported by MOST (Grant No. 2013CB834602), NSFC (Grant No. 21273213), and FRFCU. We also thank an anonymous reviewer for the comments on our previous manuscript.

[1]T. Jungwirth, J. Wunderlich, and K. Olejnik, Nat. Mater. **11**, 382 (2012); J. J. Deisz and T. E. Kidd, Phys. Rev. Lett. **107**, 277003 (2011).
[2]W. G. Richards, H. P. Trivedi, and D. L. Cooper, *Spin-Orbit Coupling in Molecules* (Clarendon Press, Oxford, 1981).
[3]D. Čubrić, A. A. Wills, J. Comer, and M. Ukai, Phys. Rev. Lett. **71**, 983 (1993).
[4]L. H. Andersen, J. H. Posthumus, O. Vahtras, H. Ågren, N. Elander, A. Nunez, A. Scrinzi, M. Natiello, and M. Larsson, Phys. Rev. Lett. **71**, 1812 (1993).
[5]H. A. Bethe and E. E. Salpeter, *Quantum Mechanics of One- and Two-Electron Atoms* (Springer-Verlag, Berlin, 1957).
[6]T. P. Rakitzis and A. J. Alexander, J. Chem. Phys. **132**, 224310 (2010).
[7]A. U. Hazi, J. Phys. B **16**, L29 (1983).
[8]Y. Le Coat, R. Azria, and M. Tronc, J. Phys. B **18**, 809 (1985).
[9]D. A. Chapman, K. Balasubramanian, and S. H. Lin, Phys. Rev. A **38**, 6098 (1988).
[10]Y. Le Coat, J.-P. Guillotin, and L. Bouby, J. Phys. B **24**, 3285 (1991).
[11]P. E. Maslen, J. Faeder, and R. Parson, Chem. Phys. Lett. **263**, 63 (1996).
[12]B. Wu, L. Xia, H.-K. Li, X.-J. Zeng, and S. X. Tian, Rev. Sci. Instrum. **83**, 013108 (2012).
[13]S. X. Tian, B. Wu, L. Xia, H.-K. Li, X.-J. Zeng, Y. Luo, and J. L. Yang, Phys. Rev. A **88**, 012708 (2013).
[14]B. Wu, L. Xia, Y.-F. Wang, H.-K. Li, X.-J. Zeng, and S. X. Tian, Phys. Rev. A **85**, 052709 (2012).
[15]L. Xia, B. Wu, H.-K. Li, X.-J. Zeng, and S. X. Tian, J. Chem. Phys. **137**, 151102 (2012).
[16]L. Xia, X.-J. Zeng, H.-K. Li, B. Wu, and S. X. Tian, Angew. Chem., Int. Ed. **52**, 1013 (2013).
[17]See supplementary material at http://dx.doi.org/10.1063/1.4862684 for the computational and experimental details and the plotting method of the angular distributions in Fig. 4.
[18]T. F. O'Malley and H. S. Taylor, Phys. Rev. **176**, 207 (1968); M. Tronc, C. Schermann, R. I. Hall, and F. Fiquet-Fayard, J. Phys. B **10**, 305 (1977).